



HAL
open science

Electrolytic phototransistor based on graphene-MoS 2 van der Waals p-n heterojunction with tunable photoresponse

Hugo Henck, Debora Pierucci, Julien Chaste, Carl H. Naylor, Jose Avila,
Adrian Balan, Mathieu G. Silly, Maria C. Asensio, Fausto Sirotti, A. T
Charlie Johnson, et al.

► **To cite this version:**

Hugo Henck, Debora Pierucci, Julien Chaste, Carl H. Naylor, Jose Avila, et al.. Electrolytic phototransistor based on graphene-MoS 2 van der Waals p-n heterojunction with tunable photoresponse. Applied Physics Letters, 2016, 109 (11), pp.113103. 10.1063/1.4962551 . hal-01438654

HAL Id: hal-01438654

<https://hal.science/hal-01438654>

Submitted on 23 Jan 2017

HAL is a multi-disciplinary open access archive for the deposit and dissemination of scientific research documents, whether they are published or not. The documents may come from teaching and research institutions in France or abroad, or from public or private research centers.

L'archive ouverte pluridisciplinaire **HAL**, est destinée au dépôt et à la diffusion de documents scientifiques de niveau recherche, publiés ou non, émanant des établissements d'enseignement et de recherche français ou étrangers, des laboratoires publics ou privés.

Electrolytic phototransistor based on graphene-MoS₂ van der Waals p-n heterojunction with tunable photoresponse

Hugo Henck¹, Debora Pierucci¹, Julien Chaste¹, Carl H. Naylor², Jose Avila³, Adrian Balan², Mathieu G. Silly³, Maria C. Asensio³, Fausto Sirotti³, A.T Charlie Johnson², Emmanuel Lhuillier^{4*} and Abdelkarim Ouerghi^{1*}

¹ Laboratoire de Photonique et de Nanostructures (CNRS- LPN), Route de Nozay, 91460 Marcoussis, France

² Department of Physics and Astronomy, University of Pennsylvania, 209S 33rd Street, Philadelphia, Pennsylvania 19104, USA

³ Synchrotron-SOLEIL, Saint-Aubin, BP48, F91192 Gif sur Yvette Cedex, France

⁴ Institut des Nanosciences de Paris, UPMC-CNRS UMR 7588, 4 place Jussieu, boîte courrier 840, 75252 Paris cedex 05, France

Abstract: Van der Waals heterostructures (vdW) obtained by stacking 2D materials offer a promising route for next generation devices by combining different unique properties in completely new artificial materials. In particular, vdW heterostructures combine high mobility and optical properties that can be exploited for optoelectronic devices. Since the p-n junction is one of the most fundamental units of optoelectronics, we propose an approach for its fabrication based on intrinsic n doped MoS₂ and p doped bilayer graphene hybrid interfaces. We demonstrate the control of the photoconduction properties using electrolytic gating which ensures a low bias operation. We show that by finely choosing the doping value of each layer, the photoconductive properties of the hybrid system can be engineered to achieve magnitude and sign control of the photocurrent. Finally, we provide a simple phase diagram relating the photoconductive behavior with the chosen doping, which we believe can be very useful for the future design of van der Waals based photodetectors.

KEYWORDS: 2D materials, p-n junctions, MoS₂- epitaxial graphene – van der Waals heterostructure, electrolyte, phototransistor

* To whom correspondence should be sent: abdelkarim.ouerghi@lpn.cnrs.fr and el@insp.upmc.fr

Introduction

Two-dimensional (2D) materials such as graphene and transition-metal dichalcogenides(TMDC) MX_2 have great potential in next-generation nano-electronic¹⁻⁴ and nano-phonic applications⁵⁻¹⁰ owing to their extraordinary fundamental physical properties¹¹.For example, the field-effect transistors based on monolayer or few-layer MoS_2 have been reported to exhibit an excellent on/off ratio and room-temperature mobility¹².The layered TMDCbased photodetectors can achieve high responsivity and fast photoresponse^{9,13}. The recent studies of growth concerning various 2D materials¹⁴⁻¹⁷ has opened the possibility to design van der Waals (vdW) heterostructures using graphene as an underlayer, which provides more opportunities for achieving desired electronic or optoelectronic properties^{3,18-24}. In fact even if graphene has exceptionally high mobility at room temperature, for optoelectronics⁹ the overall low absorption of a single carbon layer ($\approx 2\%$) and the absence of band gap implies that graphene needs to be combined with some semiconductor compounds. Its coupling with TMDC is of utmost interest for optoelectronic devices and in particular for photodetection^{9,13,25,26}.

This quest to revisit semiconductor electronicsraises the question on the possibility to design elementary devices such as light sources, diodes and photodetectors from 2D materials. In addition the obtained devices need to stay compatible with existing driving technologies and consequently need to be operated at fairly low bias.To design such devices, control of the carrier density of the system is highly desirable since it can further be used as a switch of the material properties. Nevertheless in Van der Waals heterostructure most of the gate effect remains based on the capacitive coupling through a thick dielectric which requires large operating biases. Here we propose to use electrolyte gating to reduce the operating bias of a graphene- MoS_2 heterojunction. We saw that its behavior can be tuned from a diode to a resistive operating mode thanks to gate bias. To understand the photoresponse of the system we use a combination of photoluminescence (PL), angle-resolved photoemission (ARPES) and ultraviolet photoemission (UPS) to probe the electronic structure and band alignment of the heterojunction. We additionally demonstrate that the magnitude and sign of the photoresponse can be controlled with Fermi level tuning.

Results and discussion

We designed a Van der Waals pn junction by stacking a p-type graphene layer with a n-type MoS₂ flake. The p-type graphene is obtained by hydrogenation of epitaxial graphene resulting from the high temperature baking of a SiC substrate^{27,28}. The latter presents several advantages, in particular the lack of a transfer step between the growth and the device design. Large (20-100µm) MoS₂ flakes are grown by CVD growth¹⁶ and then further deposited on the graphene substrate thanks to a wet transfer step. More details about the growth and Van der Waals heterostructure preparation are given in the SI. Metallic contacts are then prepared by e beam lithography. One of the electrodes is directly in contact with the bottom graphene layer while the second is only connected to the MoS₂. With such geometry we are sure to only probe the vertical transport through the heterostructure. A schematic and a microscopy image of the device are given in Figure 1(a) and (b). Using Raman spectroscopy we ensure that the MoS₂ layer is indeed a monolayer^{29,30} and the low magnitude of the graphene D band confirms the low density of defect with the graphene, see Figure 1(c). Furthermore, X-Ray photoemission (Figure S2) confirms the absence of oxidation for both the carbon and MoS₂³¹⁻³³.

We observe that in absence of gating the I-V curves are linear (*i.e.* no rectifying behavior is observed) and the system is strongly photoresponsive (Figure 1(d)). The illumination leads to an increase of the slope of the I-V curve and no photovoltaic behaviors are observed (*i.e.* the current is zero at 0V, whatever the illumination), which is a typical behavior for a photoconductive system. Under a continuous illumination with a 405 nm laser and by tuning the output power from 1 to 50 mW, we observe a photocurrent ranging from 60 to 600 nA (under 1V bias). The dependence of the current with respect to irradiance is also linear (inset of Figure 1(d)). As the spot area of the laser is 1 mm² and the size of our MoS₂ of about 1400 µm² we can therefore estimate a minimum value of the responsivity R of our p-n heterojunction using the formula $R = I_{PC}/P_{light}$ where I_{PC} is the photogenerated current and P_{light} is the incident light on the active photosensor. In our case we obtain responsivity as high as 14 mA/W^{13,19}. The responsivity value is currently limited by the low absorption of the MoS₂ and by loss within the gating electrolyte. The external quantum efficiency, EQE, has been estimated at about 4.3% using the formula $EQE = \frac{hv}{e}R$. Since the absorption of a single MoS₂ layer at this energy ($\approx 3\text{eV}$) is around 6%¹³, we can estimate the photoconductance gain (ratio of the EQE by the absorption) in this system to be 0.7. This large gain value suggests an efficient charge transport in the 2D layer.

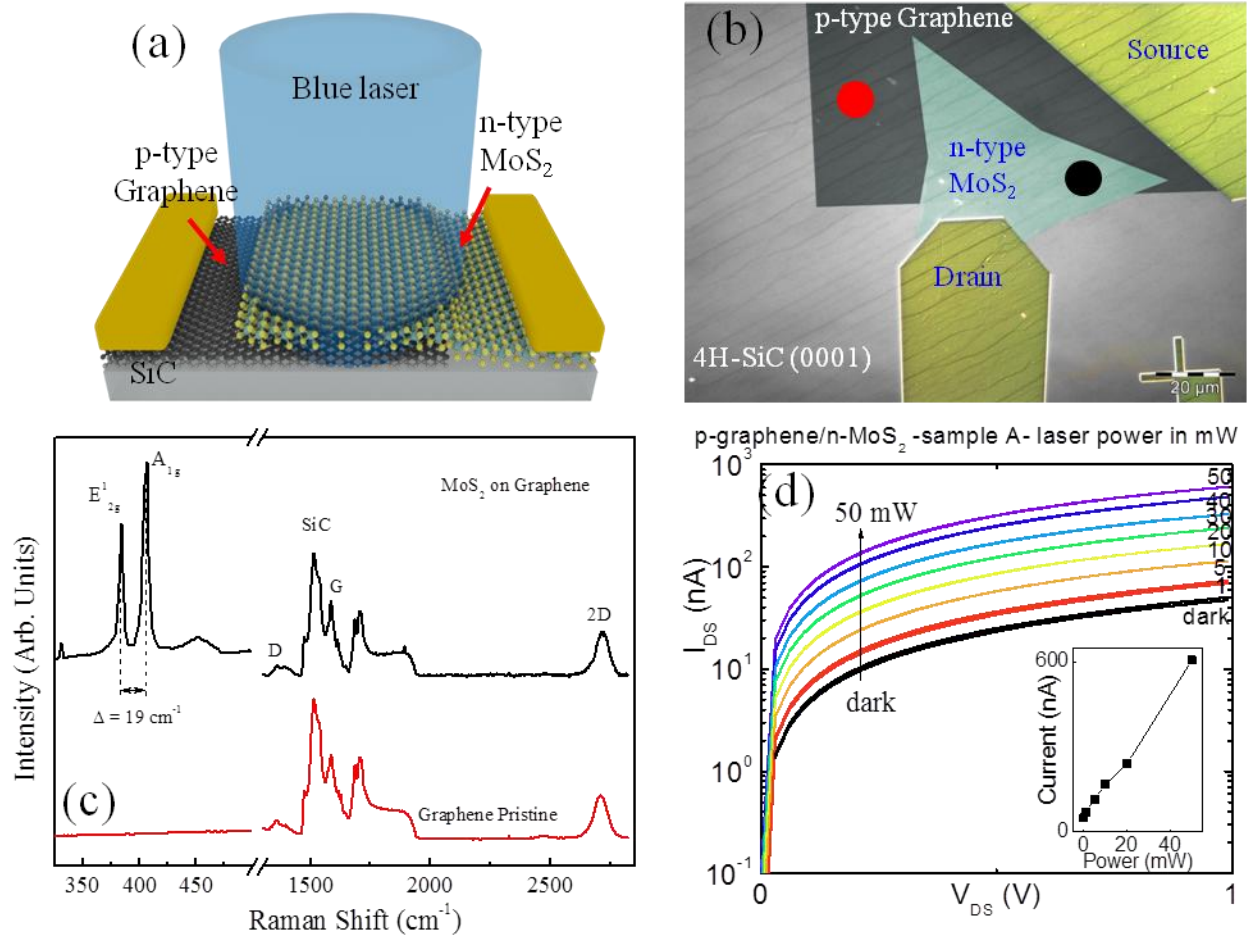


Figure 1: Schematic representation (a) and optical image (b) of the p-type graphene/n-type MoS₂ p-n junction under illumination. On part (b) the black and red spot indicates where the Raman spectrums of part c have been acquired. (c) Raman spectra of pristine graphene and MoS₂ decorated graphene. (d) Current as a function of voltage for the graphene MoS₂ junction under dark condition and under different power of illumination ($\lambda = 405$ nm). There is no gate for this measurement. The inset is the current as a function of the incident light power ($\lambda = 405$ nm), the drain source voltage is set at 1V.

In the following we implement ion-gel³⁴⁻³⁷ as a strategy to control the Fermi level in the heterostructure. Compared to conventional dielectrics for which the gate capacitance is proportional to the ratio of the dielectric constant over the dielectric thickness, in electrolytes the capacitance is driven by the size of the ionic double layer. Using small cations such as Li⁺ (100 pm in size) we expect a much larger gate capacitance. As a result, the same carrier density modulation can be obtained using a reduced operating

gate bias³⁸. Electrolyte gating of Van der Waals heterostructures is currently driving a lot of interest and it has been used to design elementary blocks for electronics³⁹ or to tune the optical properties of the heterostructures^{40,41}. Under such control of the Fermi level, we obtain a strong current modulation with on-off ratio close to 4 orders of magnitude (Figure 2(a) and S6). Thanks to the electrolyte gating this modulation is obtained while the gate bias remains limited to the ± 1.25 V range and while keeping the leakage current low (\approx nA). As previously observed^{19,20}, the conductance rises under positive gate bias (*i.e.* electron injection) which is the expected behavior for a n-type system. In this case, the large current modulation can be mostly attributed to the Fermi level tuning within the semiconductor. The subthreshold slope relates the change of current with the applied gate bias. Its value is a good indicator of the presence of unpassivated surface charges. We measure a value as small as 160 meV/decade at room temperature. This value is typically only twice as large as the thermodynamic limit $\frac{k_b T}{e} \log(10)$ (with k_b the Boltzmann constant, T the temperature and e the proton charge), which reflects the presence of a small amount of unpassivated charge at the interface with electrolyte. Nevertheless, such small subthreshold slope is typically one order of magnitude smaller than the value obtained with the conventional back gating method². We observe that the shape of the I-V curve (drain current as a function of drain source bias) is strongly dependent on the gate bias¹⁹. Under negative gate bias, the expected rectifying behavior from the p-n junction is observed (Figure 2(b)). On the other hand, when the gate bias is switched to positive bias, the I-V becomes linear as in absence of gating (Figure 1(d) and Figure 2(b)). We attribute this change to the chosen value of doping for MoS₂ and graphene. While holes are injected ($V_{GS} < 0$) the p character of the graphene is reinforced and the strong initial n type doping ($8 \times 10^{12} \text{cm}^{-2}$) is sufficient to preserve the p-n junction formation. In this regime we obtain a diode-like IV curve and the conductance is low, around 0V. *A contrario*, due to its very light p character, electron injection ($V_{GS} > 0$) makes that graphene almost intrinsic and the rectifying behavior is suppressed. Therefore, a very conductive n-n junction is formed and presents an ohmic behavior.

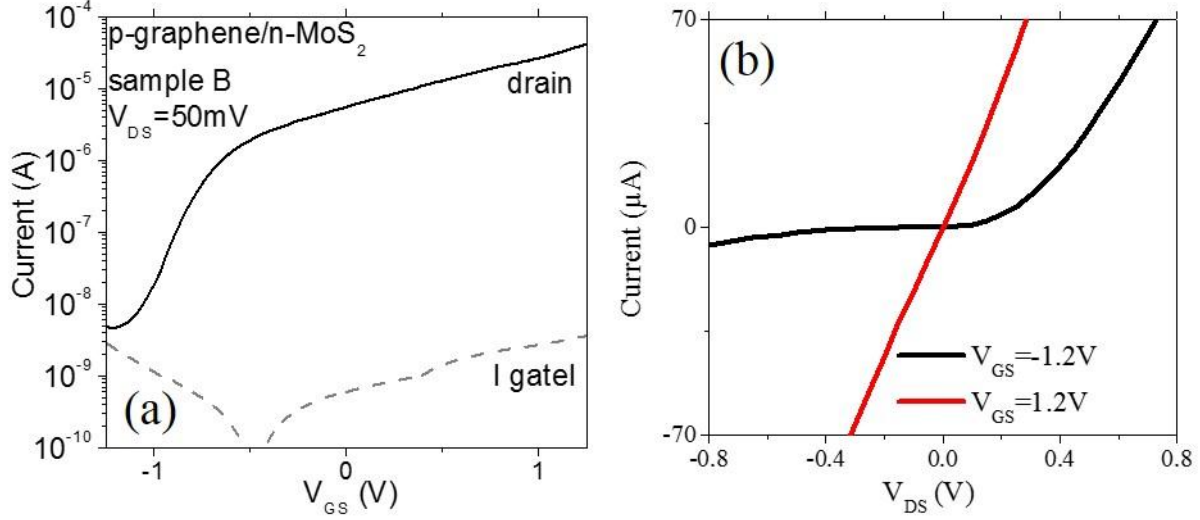


Figure 2 (a) Transfer curve (drain and gate current) as a function of gate bias for the graphene MoS₂ junction. (b) IV curve under two values of the gate bias for the graphene MoS₂ junction under different gate bias. All measurements are made at room temperature.

To understand the observed behavior and the following photocurrent measurements, we then need to probe the electronic structure of the heterostructure and the relative band offset between the components. From PL measurements, we can estimate the band gap of the MoS₂ layer to be 1.83 eV. As shown in [Figure S2\(a\)](#), this value corresponds to the main transition peak in the spectrum (named A) arising from the direct inter-band recombination at the K- point of the Brillouin zone of the photogenerated electron-hole pairs⁴²⁻⁴⁴. However it should be noted that using STS the obtained electronic band gap is 2 eV⁴⁵, which is 0.17 eV larger than the optical band gap due to the high excitonic binding energy for this 2D system. Complementarily UPS measurements give us the energy distance between the valence band of MoS₂ and the Fermi level as well as the Fermi level and vacuum level. These two values are respectively 1.25 eV and 4.47 eV, see [Figure S2\(c\)](#) and [\(d\)](#). This first value confirms the n type nature of the MoS₂ layer since the Fermi level is located at $\approx 2/3$ of the band edge energy. Finally using ARPES we can estimate the energy distance from the valence band maximum to minimum conduction band of the bilayer graphene. A linear extrapolation of the bands gives us a value of 0.25 eV, see [Figure S2\(b\)](#), which confirm the p type doping of bilayer graphene. According to the measured Fermi velocity ($v_F \approx 1.1 \times 10^6$ m/s) we can estimate the hole doping level to be 3.8×10^{12} cm⁻². These four measurements together let us propose a model for the electronic structure, see [Figure S2\(e\)](#).

We then investigated the photoresponse of the electrolytic transistor. Under negative gate bias ($V_{GS} = -1.25V$), the electrolyte gating injects hole within the system, which depletes the n-type MoS_2 from its electrons. As a result, the system gets poorly conductive under dark conditions and large photocurrent modulation is observed (Figure 3(a)). In fact this regime is the one leading to the strongest photocurrent modulation in Figure 3(a-f). In this configuration the Fermi level of the p-n junction lies close to the middle of the band gap energy of MoS_2 , while the graphene p character is reinforced⁴⁶. When the gate bias remains negative but gets closer to 0V, the Fermi level is pushed closer to the conduction band of MoS_2 , thus more carriers are thermally activated and the conductance in the dark is now significantly enhanced, see Figure 3(d). Under illumination we observe a positive photoresponse, see Figure 3(c), very similar to the one observed for the pristine MoS_2 device¹⁰. Once the gate bias is switched to a positive value, the photo-behavior is strongly affected and we now observe both positive and negative photoresponses depending on the incident light power (Figure 3(e) and (f)). As the Fermi level passes over the MoS_2 valence band, hole-trapping in band-tail states is one of the mechanisms playing a role in the photocurrent generation⁴⁷. Under strong electron injection, the charge modulation resulting from illumination is now small compared to the gate-induced carrier density. We speculate that the negative photocurrent no longer results from a change of the carrier density but rather from a drop of the mobility. Indeed, the hole minority carrier is more likely to recombine with an electron if the electron carrier density is high. Indeed in this strongly n-doped MoS_2 , photogenerated holes will behave as recombination centers for electrons, which reduces their mobility.

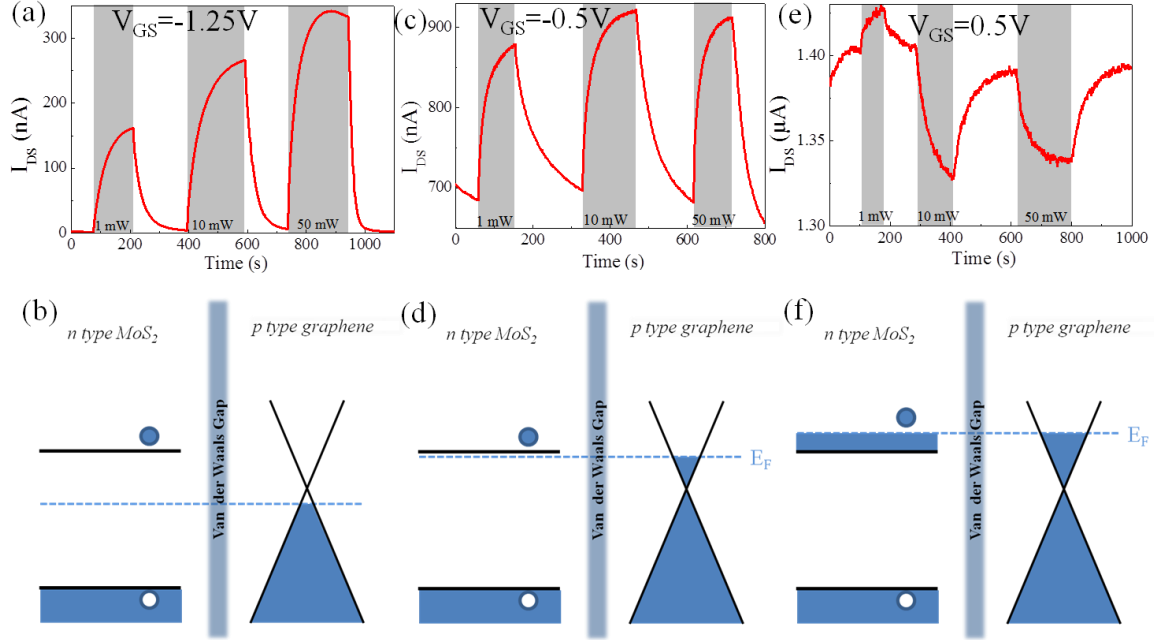


Figure 3 (a) Time trace of the current under pulse of illumination of different incident light power ($\lambda = 405 \text{ nm}$) for a gate bias of $V_{GS} = -1.25 \text{ V}$, (b) is the scheme of the associated band structure, (c) and (d) are the same graph under $V_{GS} = -0.5 \text{ V}$, while (e) and (f) are the same set of data for $V_{GS} = 0.5 \text{ V}$. All the data are measured for $V_{DS} = 10 \text{ mV}$.

We can now summarize our observations regarding vertical transport in the graphene-MoS₂ heterostructure (Figure 4(a)) in which the electron transfer from the semiconductor to the semimetal is the transport limiting factor. We can plot a phase diagram (Figure 4(b)), which summarizes the type of photoresponse expected for the device as a function of the MoS₂ and graphene layer doping. Three main phases have been observed. The first is a “diode”-like phase, which requires sufficiently high p-doping for the graphene. Next is an intermediate phase where graphene is lightly p doped and behaves more or less like a contact. Finally, when the Fermi level is brought in the conduction band, a negative ohmic photoresponse is obtained, as a result of holes acting as a recombination center in the strongly n-doped MoS₂.

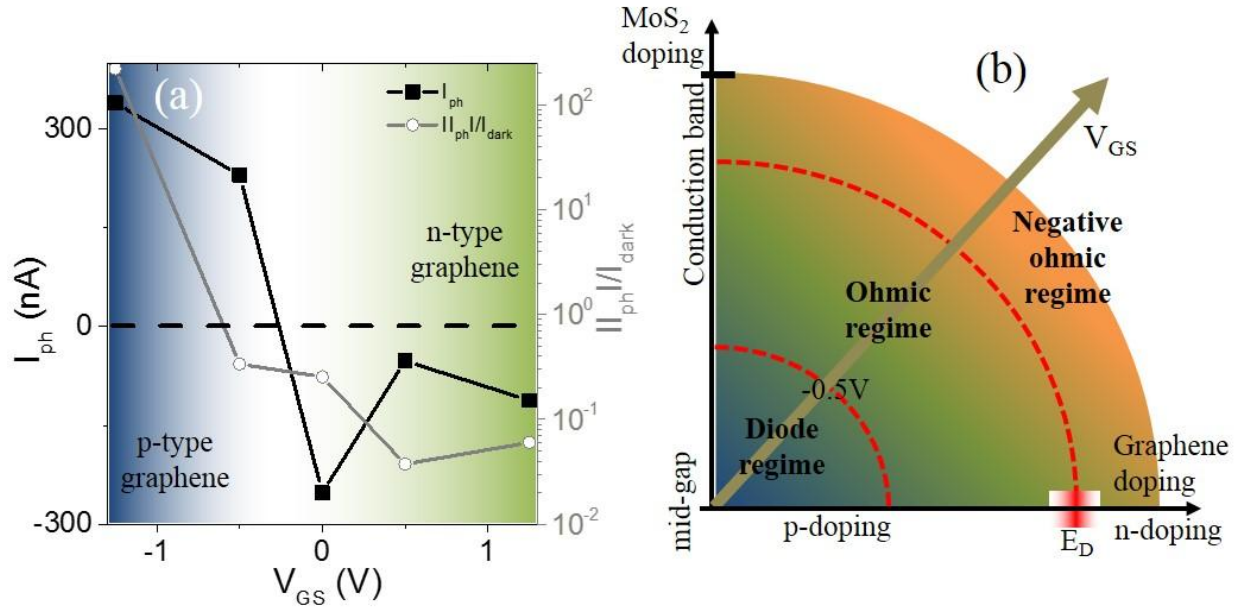


Figure 4:(a) Photocurrent (total current minus dark current) and photocurrent divided by the dark current as a function of gate voltage for the p-type graphene/n-type MoS₂ pn junction. $V_{DS}=10mV$ and the incident light power is 50mW, (b) Phase diagram of photoresponse behavior of the pn junction with respect to the doping of both graphene and MoS₂.

Conclusion

In conclusion, we have fabricated a p-n junction from vertically stacked p-doped bilayer graphene and n-doped MoS₂. We have provided band alignment for the p-type bilayer graphene/n-type monolayer MoS₂ and investigated its structural and electronic properties. The high-resolution XPS and ARPES measurements demonstrate the absence of any inter-diffusion and contamination between MoS₂ and the graphene layer, and indicates that the MoS₂ and graphene layer exhibits an n- and p- type behaviour. We propose a geometry of van der Waals phototransistors based on electrolyte gating. We demonstrate that the control of the carrier density allows fine-tuning of the magnitude and the sign of the photoresponse while keeping the operating bias low. We propose a doping phase diagram for the design of a graphene-MoS₂ heterostructure which highlights the importance of a careful choice for the doping of each layer in the final obtained optoelectronic behavior.

Supplementary material

See supplemental material at [URL will be inserted by AIP] for additional data about the XPS, measurement of the band diagram and additional device and transport data.

Acknowledgements: This work was supported by the ANR SUPERTRAMP and H2DH grants. This work is supported by a public grant overseen by the French National Research Agency (ANR) as part of the “Investissements d’Avenir” program (reference: ANR-10-LABX-0035, Labex NanoSaclay and ANR-11-IDEX-0004-02, labex MATISSE). C.H.N. and A.T.C.J. acknowledge support from the National Science Foundation EFRI-2DARE program, grant number ENG- 1542879. Photoemission experiments have been carried out at the Antares beamline of the Synchrotron SOLEIL, this institution is supported by the Centre National de la Recherche Scientifique (CNRS) and the Commissariat à l’Energie Atomique et aux Energies Alternatives (CEA), France.

Competing financial interests: The authors declare no competing financial interests.

References

- ¹ E. Kaxiras, J. Kong, and H. Wang, *Nano Lett.* **14**, 3055 (2014).
- ² H. Tian, Z. Tan, C. Wu, X. Wang, M.A. Mohammad, D. Xie, Y. Yang, J. Wang, L.-J. Li, J. Xu, and T.-L. Ren, *Sci. Rep.* **4**, 5951 (2014).
- ³ L. Britnell, R. V. Gorbachev, R. Jalil, B.D. Belle, F. Schedin, a. Mishchenko, T. Georgiou, M.I. Katsnelson, L. Eaves, S. V. Morozov, N.M.R. Peres, J. Leist, a. K. Geim, K.S. Novoselov, and L. A. Ponomarenko, *Science* **335**, 947 (2012).
- ⁴ J.Y. Kwak, J. Hwang, B. Calderon, H. Alsalman, N. Munoz, B. Schutter, and M.G. Spencer, *Nano Lett.* **14**, 4511 (2014).
- ⁵ F. Xia, H. Wang, D. Xiao, M. Dubey, and A. Ramasubramaniam, *Nat. Photonics* **8**, 899 (2014).
- ⁶ W. Zhang, C.-P. Chuu, J.-K. Huang, C.-H. Chen, M.-L. Tsai, Y.-H. Chang, C.-T. Liang, J.-H. He, M.-Y. Chou, and L.-J. Li, *Sci. Rep.* **4**, 1 (2014).
- ⁷ Pierucci, D.; Sediri, H.; Hajlaoui, M.; Velez-Fort, E.; Dappe, Y. J.; Silly, M. G.; Belkhou, R.; Shukla, A.; Sirotti, F.; Gogneau, N.; Ouerghi, A. *Nano Res.* **2015**, 8 (3), 1026–1037.
- ⁸ X. Li, J. Wu, N. Mao, J. Zhang, Z. Lei, Z. Liu, and H. Xu, *Carbon* **92**, 126 (2015).
- ⁹ F.H. Koppens, T. Mueller, P. Avouris, a C. Ferrari, M.S. Vitiello, and M. Polini, *Nat Nanotechnol* **9**, 780 (2014).
- ¹⁰ O. Lopez-Sanchez, D. Lembke, M. Kayci, A. Radenovic, and A. Kis, *Nat. Nanotechnol.* **8**, 497 (2013).
- ¹¹ K.S. Novoselov, V.I. Fal’ko, L. Colombo, P.R. Gellert, M.G. Schwab, and K. Kim, *Nature* **490**, 192 (2012).
- ¹² B. Radisavljevic, a Radenovic, J. Brivio, V. Giacometti, and A. Kis, *Nat. Nanotechnol.* **6**, 147 (2011).
- ¹³ W. Zhang, C.-P. Chuu, J.-K. Huang, C.-H. Chen, M.-L. Tsai, Y.-H. Chang, C.-T. Liang, Y.-Z. Chen, Y.-L. Chueh,

- J.-H. He, M.-Y. Chou, and L.-J. Li, *Sci. Rep.* **4**, 3826 (2014).
- ¹⁴ P. Miró, M. Audiffred, and T. Heine, *Chem. Soc. Rev.* **43**, 6537 (2014).
- ¹⁵ E. Lhuillier, S. Pedetti, S. Ithurria, B. Nadal, H. Heuclin, and B. Dubertret, *Acc. Chem. Res.* **48**, 22 (2015).
- ¹⁶ G.H. Han, N.J. Kybert, C.H. Naylor, B.S. Lee, J. Ping, J.H. Park, J. Kang, S.Y. Lee, Y.H. Lee, R. Agarwal, and a T.C. Johnson, *Nat. Commun.* **6**, 6128 (2015).
- ¹⁷ Y.-C. Lin, N. Lu, N. Perea-Lopez, J. Li, Z. Lin, X. Peng, C.H. Lee, C. Sun, L. Calderin, P.N. Browning, M.S. Bresnehan, M.J. Kim, T.S. Mayer, M. Terrones, and J.A. Robinson, *ACS Nano* **8**, 3715 (2014).
- ¹⁸ L. Britnell, R.M. Ribeiro, A. Eckmann, R. Jalil, B.D. Belle, A. Mishchenko, Y. Kim, R. V Gorbachev, T. Georgiou, S. V Morozov, A.N. Grigorenko, A.K. Geim, C. Casiraghi, A.H.C. Neto, and K.S. Novoselov, *Science***340**, 1311 (2013).
- ¹⁹ S. Rathi, I. Lee, D. Lim, J. Wang, Y. Ochiai, N. Aoki, K. Watanabe, T. Taniguchi, G.-H. Lee, Y.-J. Yu, P. Kim, and G.-H. Kim, *Nano Lett.* **15**, 5017 (2015).
- ²⁰ C.J. Shih, Q.H. Wang, Y. Son, Z. Jin, D. Blankshtein, and M.S. Strano, *ACS Nano* **8**, 5790 (2014).
- ²¹ C.-H. Lee, G.-H. Lee, A.M. van der Zande, W. Chen, Y. Li, M. Han, X. Cui, G. Arefe, C. Nuckolls, T.F. Heinz, J. Guo, J. Hone, and P. Kim, *Nat. Nanotechnol.* **9**, 676 (2014).
- ²² K.T. Lam, G. Seol, J. Guo, *Appl. Phys. Lett.* **105**, 013112 (2014).
- ²³ T. Roy, M. Tosun, J.S. Kang, A.B. Sachid, S.B. Desai, M. Hettick, C.C. Hu, and A. Javey, *ACS Nano* **8**, 6259 (2014).
- ²⁴ D. Pierucci, H. Henck, C.H. Naylor, H. Sediri, E. Lhuillier, A. Balan, J.E. Rault, Y.J. Dappe, F. Bertran, P. Le Fèvre, A.T.C. Johnson, and A. Ouerghi, *Sci. Rep.* **6**, 26656 (2016).
- ²⁵ W.J. Yu, Y. Liu, H. Zhou, A. Yin, Z. Li, Y. Huang, and X. Duan, *Nat. Nanotechnol.* **8**, 952 (2013).
- ²⁶ M. Buscema, J.O. Island, D.J. Groenendijk, S.I. Blanter, G.A. Steele, H.S. van der Zant, and A. Castellanos-Gomez, *Chem Soc Rev* **44**, 3691 (2015).
- ²⁷ E. Velez-fort, C. Mathieu, E. Pallecchi, M. Pigneur, M.G. Silly, R. Belkhou, M. Marangolo, A. Shukla, F. Sirotti, A. Ouerghi, *ACS Nano* **6**, 10893 (2012).
- ²⁸ E. Pallecchi, F. Lafont, V. Cavaliere, F. Schopfer, D. Mailly, W. Poirier, and A. Ouerghi, *Sci. Rep.* **4**, 4558 (2014).
- ²⁹ H. Li, Q. Zhang, C.C.R. Yap, B.K. Tay, T.H.T. Edwin, A. Olivier, and D. Baillargeat, *Adv. Funct. Mater.* **22**, 1385 (2012).
- ³⁰ C. Lee, H. Yan, L.E. Brus, T.F. Heinz, K.J. Hone, and S. Ryu, *ACS Nano* **4**, 2695 (2010).
- ³¹ A. Ouerghi, R. Belkhou, M. Marangolo, M.G. Silly, S. El Moussaoui, M. Eddrief, L. Largeau, M. Portail, and F. Sirotti, *Appl. Phys. Lett.* **97**, 161905 (2010).
- ³² K. V. Emtsev, F. Speck, T. Seyller, L. Ley, and R. J.D., *Phys. Rev. B* **77**, 155303 (2008).
- ³³ P.D. Fleischauer and J.R. Lince, *Tribol. Int.* **32**, 627 (1999).
- ³⁴ E. Lhuillier, S. Ithurria, A. Descamps-Mandine, T. Douillard, R. Castaing, X.Z. Xu, P.-L. Taberna, P. Simon, H. Aubin, and B. Dubertret, *J. Phys. Chem. C* **119**, 21795 (2015).

- ³⁵ E. Lhuillier, A. Robin, S. Ithurria, H. Aubin, and B. Dubertret, *Nano Lett.* **14**, 2715 (2014).
- ³⁶ Y. Zhang, J. Ye, Y. Yomogida, T. Takenobu, and Y. Iwasa, *Nano Lett.* **13**, 3023 (2013).
- ³⁷ G. Froehlicher and S. Berciaud, *Phys. Rev. B* **91**, 205413 (2015).
- ³⁸ A. Robin, E. Lhuillier, X.Z. Xu, S. Ithurria, H. Aubin, A. Ouerghi, and B. Dubertret, *Sci. Rep.* **6**, 24009 (2016).
- ³⁹ Y. Choi, J. Kang, D. Jariwala, M.S. Kang, T.J. Marks, M.C. Hersam, and J.H. Cho, *Adv. Mat.* **28**, 3742 (2016).
- ⁴⁰ Sediri, H.; Pierucci, D.; Hajlaoui, M.; Henck, H.; Patriarche, G.; Dappe, Y. J.; Yuan, S.; Toury, B.; Belkhou, R.; Silly, M. G.; Sirotti, F.; Boutchich, M.; Ouerghi, A. *Sci. Rep.* **2015**, *5*, 16465.
- ⁴¹ Y. Li, C.-Y. Xu, J.-K. Qin, W. Feng, J.-Y. Wang, S. Zhang, L.-P. Ma, J. Cao, P.A. Hu, W. Ren, and L. Zhen, *Adv. Func. Mat.* **26**, 293 (2016).
- ⁴² A. Splendiani, L. Sun, Y. Zhang, T. Li, J. Kim, C.-Y. Chim, G. Galli, and F. Wang, *Nano Lett.* **10**, 1271 (2010).
- ⁴³ G. Eda, H. Yamaguchi, D. Voiry, T. Fujita, M. Chen, and M. Chhowalla, *Nano Lett.* **11**, 5111 (2011).
- ⁴⁴ K.F. Mak, C. Lee, J. Hone, J. Shan, and T.F. Heinz, *Phys. Rev. Lett.* **105**, 136805 (2010).
- ⁴⁵ X. Liu, I. Balla, H. Bergeron, G.P. Campbell, M.J. Bedzyk, and M.C. Hersam, *ACS Nano* **10**, 1067 (2016).
- ⁴⁶ D. Jariwala, V.K. Sangwan, C.-C.C.-C. Wu, P.L. Prabhumirashi, M.L. Geier, T.J. Marks, L.J. Lauhon, and M.C. Hersam, *Proc. Natl. Acad. Sci.* **110**, 18076 (2013).
- ⁴⁷ M.M. Furchi, D.K. Polyushkin, A. Pospischil, and T. Mueller, *Nano Lett.* **14**, 6165 (2014).